Check for updates

Fucoidan-mediated green synthesis of palladium nanoparticles as a recyclable catalyst for Heck coupling and alkyne reduction in pheromone synthesis

Van-Dung Le, [ID] †[ab] Minh-Vuong Phan,†[ab] Nhat-Minh Phan,[ab]
Nguyen-Khanh-Vu Ngo,[a] Thi-Yen-Nghi Le,[a] Truc-Vy Mai,[a] Duc-Huy Pham,[a]
Minh-Trong Tran,[a] Minh-Ty Nguyen,[a] Thi-Cam-Thu Nguyen, [ID] [a]
Thanh-Danh Nguyen, [ID] [ab] Dinh-Tri Mai,[ab] Thi-Ngoc-Mai Tran,[c]
Thi-Thanh-Tu Nguyen,[d] Hoang-Nhu-Khanh Huynh[e] and Chi-Hien Dang [ID] *[ab]

The development of sustainable routes for metallic nanocatalysts remains challenging due to the reliance on toxic reagents and harsh synthesis conditions. To address this, a green and efficient method was established for the preparation of palladium nanoparticles (PdNPs@Fu) using fucoidan, a naturally occurring polysaccharide with several hydroxyl and sulfate groups as a stabilizing and reducing agent. Fucoidan can rapidly reduce Pd^{2+} to Pd^0 in aqueous medium under microwave irradiation (450 W, 10 min). The resulting PdNPs@Fu exhibited uniform crystalline nanoparticles (sizes ranging from 2–6 nm and an average diameter of 3.83 ± 0.09 nm), with long-term colloidal stability over 30 days. Catalytic studies demonstrated remarkable activity in model organic transformations: the Heck coupling (93% yield, 84% after five cycles) and the selective semi-hydrogenation of alkynes to (Z)-alkenes (94% yield, 85% retained activity). Notably, the catalyst afforded an overall yield of 78% in the synthesis of the sweet potato weevil (*Cylas formicarius*) pheromone. This research introduces a green synthesis strategy of PdNPs, integrating nanotechnology with efficient pheromone synthesis for insect control.

1 Introduction

The development of environmentally friendly and innovative materials has emerged as a global priority in the pursuit of sustainable development, particularly in the field of catalytic nanomaterials. Conventional synthetic approaches often rely on toxic organic solvents such as DMF, DMSO, ethanol, and acetonitrile, which pose serious risks to both human health and the environment. Consequently, green synthetic strategies that employ eco-friendly solvents like water and bio-based

precursors under microwave-assisted conditions offer a promising and sustainable alternative to traditional methods.[1–4]

Fucoidan, a natural sulfated polysaccharide derived from brown seaweed, is well known as a reducing and stabilizing agent due to its water solubility and abundance of hydroxyl and sulfate groups. It has been widely applied in the synthesis of various metal nanoparticles. As an illustration, gold nanoparticles (AuNPs) with particle sizes of around 4–8 nm were produced utilizing fucoidan that was isolated from *Sargassum cinereum* and *Turbinaria decurrens*.[5–8] More recently, fucoidan was used to produce silver nanoparticles (AgNPs) with an average size of 180 nm and a 5% Ag content.[9] In another study, fucoidan-assisted microwave synthesis produced AgNPs with an average diameter of 59.5 ± 1.46 nm.[10] Notably, the combination of fucoidan with chitosan as a biopolymer coating yielded AgNPs with an average size of 50 nm.[11] Furthermore, a green synthesis approach employing fucoidan resulted in AgNPs with particle sizes ranging from 4 to 45 nm.[12] Fucoidan has been used as a biopolymer template to create mesoporous platinum nanoparticles (HM-PtNPs) with sizes ranging from 2 to 5 nm, in addition to silver and gold nanoparticles. These nanoparticles showed catalytic activity in the hydrogen evolution reaction (HER) that was comparable to that of commercial Pt/C catalysts,

[a]Institute of Advanced Technology, Vietnam Academy of Science and Technology, 1B TL29 Street, An Phu Dong Ward, Ho Chi Minh City, Vietnam. E-mail: dangchihien@gmail.com

[b]Graduate University of Science and Technology, Vietnam Academy of Science and Technology, 18 Hoang Quoc Viet, Nghia Do Ward, Hanoi, Vietnam

[c]Institute of Applied Sciences, HUTECH University, Ho Chi Minh City, Vietnam 475A Dien Bien Phu Street, Thanh My Tay Ward, Ho Chi Minh City, Vietnam

[d]Faculty of Applied Technology, Van Lang School of Technology, Van Lang University, Ho Chi Minh City, Vietnam

[e]Institute of Oceanography, Vietnam Academy of Science and Technology, 01 Cau Da, Nha Trang, Khanh Hoa, Vietnam

† These authors contributed equally to this work.

but they also showed better stability and lower costs.[13] Another study developed fucoidan–cis-platin nanocomposites, where fucoidan acted not only as a carrier but also enhanced cisplatin delivery to cancer cells.[14–16] These findings highlight that fucoidan is more than an effective biological stabilizer; it represents a versatile platform with dual catalysis applications in organic synthesis.

For the green, easy, efficient, and economical synthesis of PdNPs, natural polysaccharides as chitosan, alginate, chitooligosaccharide, β-cyclodextrin (β-CD), carboxymethyl cellulose (CMC), and plant extracts have been used extensively as reducing and stabilizing agents in recent years.[17–23] The resultant PdNP catalysts usually have a uniform shape, great stability, good dispersibility, and tiny particle sizes (2–10 nm). Consequently, they have shown excellent catalytic performance in C–C coupling reactions such as Suzuki, Sonogashira, and Heck.[19,22] For instance, at room temperature, *Sapindus mukorossi* extract-derived PdNPs effectively catalyzed the Suzuki process with yields higher than 90%.[22] Similarly, PdNPs derived from *Asterarcys* sp. and chitosan demonstrated high reusability while retaining catalytic efficiency.[20] PdNPs made more recently using β-cyclodextrin and carboxymethyl cellulose had particle diameters of 4–6 nm and were efficient catalysts for alkyne reactions and Sonogashira coupling, both of which produced yields more than 90%.[24] However, these studies have primarily focused on common polysaccharides or plant-derived extracts. In contrast, unique marine polysaccharides, such as fucoidan with its distinct chemical structures and abundant functional groups, remain largely unexplored. This disparity demonstrates fucoidan's promise as a cutting-edge, environmentally friendly platform for PdNPs' green synthesis and catalytic uses.

PdNPs can function as excellent heterogeneous catalysts for the reduction process of alkyne to (Z)-alkene with great selectivity without the need for molecular hydrogen, as several recent studies have shown.[25–27] Notably, Ballesteros-Soberanas *et al.* demonstrated that the catalyst's catalytic efficiency can still effectively and selectively catalyze the semi-reduction of (Z)-alkene with Pd.[26] At the same time, Shi *et al.* exploited water as a hydrogen source, enabling an environmentally friendly and selective transformation.[27] In our recent studies, *Cyclea barbata* pectin-derived PdNPs, as well as polysaccharides such as β-cyclodextrin (β-CD) and carboxymethyl cellulose (CMC), also exhibited high efficiency in the selective reduction of alkynes to (Z)-alkenes.[23,24] These findings underscore the potential of PdNPs in green and sustainable alkyne semi-hydrogenation reactions. This gap is particularly significant, since selective alkyne hydrogenation is a key step in the synthesis of (Z)-alkene pheromones without molecular hydrogen, where controlling the predominance of the (Z)-isomer is essential to ensure the biological activity of pheromone molecules.[24]

This study presents a sustainable, microwave-assisted synthesis strategy for the fabrication of fucoidan-based palladium nanoparticles (PdNPs@Fu) in an aqueous environment. This is a rapid, economical, and completely "green" route, in which fucoidan plays a dual role as a reducing agent and a stabilizer without the addition of any toxic chemicals. The breakthrough of this study lies in the superiority in structure

and catalytic performance of PdNPs@Fu compared to previous material systems such as PdNPs@pectin[23] or PdNPs@β-CD/CMC.[24] The novelty of this research is highlighted by three main aspects.

First, in terms of chemical nature, the high density of negatively charged sulfate groups ($-SO_3^-$) on the fucoidan backbone forms a stable electrostatic shell, enabling effective control of ultra-small particle sizes, unlike the carboxylate group ($-COO^-$) in pectin. Second, regarding atom economy, PdNPs@Fu shows superior metal utilization efficiency, requiring lower palladium loading than the PdNPs@pectin system to achieve similar reaction efficiencies. Finally, in catalytic performance, this material demonstrates significant activity in key reactions such as Heck coupling and alkyne semi-hydrogenation, highlighting its potential in natural product synthesis and pheromone development. These aspects collectively enhance the scientific understanding of this innovative approach.

2 Materials and methods

2.1. Materials

The key reagents, namely 1-decyne (98%), 2-(2-bromoethoxy) tetrahydro-2*H*-pyran (99%), *n*-butyl lithium (2.5 M in cyclohexane), 2-(2-bromoethoxy)tetrahydro-2*H*-pyran (96%), 2-butyn-1-ol (98%), Pd(OAc)$_2$ (47% Pd), *p*-toluenesulfonic acid monohydrate (99%), *trans*-crotonyl chloride (90%), and fucoidan (≥95%), were purchased from Acros (Belgium). The compound 2-(but-3-yn-1-yloxy)tetrahydro-2*H*-pyran was synthesized following a previously reported procedure.[24]

2.2. Synthesis of PdNPs@Fu

To a 250 mL round-bottom flask with 135.35 mL of distilled water, add 0.1223 g of fucoidan, and ultrasonicate the mixture is ultrasonicated for 15 minutes. Dissolve 90 mg of Pd(OAc)$_2$ in 6 mL of ethanol at a ratio of 15 mg mL^{-1}, then add it to the mixture and continue sonication for 30 minutes to obtain a homogeneous solution. Following ultrasound, the yellow solution is heated for 10 min at 450 W in a microwave, obtaining a black solution, indicating the successful reduction of Pd^{2+} ions to PdNPs. The black solution is separated and purified using centrifugation at 12 000 rpm, 4 °C, and 15 min to produce PdNPs@Fu (repeated three times). The synthesized nanomaterial powder is then lyophilized at −78 °C for 24 hours and stored at room temperature for future usage.

2.3. Physicochemical characterization of PdNPs@Fu

UV-vis spectroscopy was carried out using a JASCO V-630 spectrophotometer (USA) over the wavelength range of 200–800 nm. FTIR and Raman spectra of fucoidan, Pd(OAc)$_2$, and PdNPs@Fu were recorded using a Bruker Tensor 27 FTIR spectrometer (Germany) and an Xplora Plus Raman spectrometer (Horiba, France), respectively. The crystal structure of PdNPs was examined *via* X-ray diffraction (XRD) using a Bruker D8 Advance diffractometer. Particle size and zeta potential of the nanocomposite in aqueous solution were measured at 25 °C with

a NanoPartica Horiba SZ-100 particle analyzer (Japan). Thermogravimetric analysis (TGA) was performed on a LabSys evo S60/58988 thermoanalyzer (Setaram, France) from 30 °C to 800 °C at a heating rate of 10 °C min^{-1} under an air atmosphere. TEM images were obtained using a Hitachi H810. Particle diameters were analyzed with ImageJ from manually selected regions to minimize bias. Size distribution histograms were fitted with a Gaussian model in OriginPro 2021 to calculate the mean diameter (d) and standard deviation (σ). ^{1}H (600 MHz) and ^{13}C (150 MHz) nuclear magnetic resonance (NMR) spectra were recorded on a Bruker Advance 600 spectrometer using CDCl$_3$ as the solvent and tetramethylsilane (TMS) as the internal reference. Gas chromatography (GC) analyses were conducted on a Shimadzu GC-MS-QP2020 system (Japan) equipped with an Rxi-5MS capillary column (30 m × 0.25 mm i.d., 0.25 μm film thickness, Shimadzu, Japan).

3 Results and discussion

3.1. Preparation of PdNPs@Fu catalyst

The overall experimental strategy is illustrated in Fig. 1. PdNPs were synthesized *via* the *in situ* reduction of Pd^{2+} ions to Pd^0 using fucoidan as both the reducing and stabilizing agent under microwave irradiation. During the reaction, fucoidan underwent partial hydrolysis, generating reducing sugars that facilitated the formation of PdNPs. The progression of nanoparticle formation was monitored and confirmed through spectroscopic and microscopic analyses, including UV-vis, FT-IR, Raman, and TEM. The synthesized PdNPs exhibited excellent catalytic activity in model organic transformations such as the Heck coupling and the selective semi-hydrogenation of alkynes. Notably, the alkyne reduction reaction was successfully applied to the synthesis of the (*Z*)-alkene pheromone of the sweet potato weevil (*Cylas formicarius*). In addition, the catalyst demonstrated good recyclability and maintained high activity after multiple reaction cycles in the same solvent system.

The UV-vis spectra (Fig. 1B) provided clear evidence for the microwave-assisted synthesis of PdNPs@Fu in aqueous medium. A strong absorption band corresponding to Pd^{2+} ions was observed in the Pd(OAc)$_2$ precursor, whereas there are no peaks in the fucoidan spectrum. Upon microwave irradiation, the absorbance in the 200–300 nm region decreased over reaction time, indicating the rapid consumption of Pd^{2+} ions from the solution phase. This consumption is attributed to the reduction of Pd^0 and the simultaneous nucleation of PdNPs stabilized by fucoidan. The successful formation of crystalline metallic Pd^0 is subsequently confirmed by XRD and Raman analyses (Section 3.2) on the isolated solid PdNPs@Fu. The near disappearance of the Pd^{2+} signals after 10 minutes indicated that the precursor was almost fully consumed, resulting in the creation of a stable colloidal dispersion. The minor rise in absorbance at 15 minutes indicates that 10 minutes is the ideal reduction duration for this procedure. Compared with conventional chemical or thermal methods, microwave irradiation offers rapid and uniform heating, accelerates ion mobility, and minimizes nanoparticle aggregation, thereby yielding smaller, more narrowly distributed PdNPs with enhanced stability.[28,29] Moreover, the dual role of fucoidan as a natural, eco-friendly polysaccharide capable of reducing Pd^{2+} while simultaneously capping the nanoparticles further enhances the green chemistry aspect of this process.[30] Taken together, the microwave-fucoidan strategy represents a simple, time-efficient, and sustainable route for preparing highly stable PdNPs with small particle size and narrow distribution, holding great promise for applications in modern heterogeneous catalysis.[31]

3.2. Physicochemical characterizations of the catalyst

The FT-IR spectra showed the high similarity between fucoidan and PdNPs@Fu (Fig. 2). A broad absorption band at around 3455 cm^{-1} is attributed to the O–H stretching vibrations of hydroxyl groups, a typical feature of polysaccharides. The absorption peak at 2932 cm^{-1} is attributed to the asymmetric aliphatic C–H stretching vibration of the carbohydrate moieties. The peak at 1630 cm^{-1} was represented for the O–C–O stretching vibration. The strong absorption at 1255 cm^{-1} is
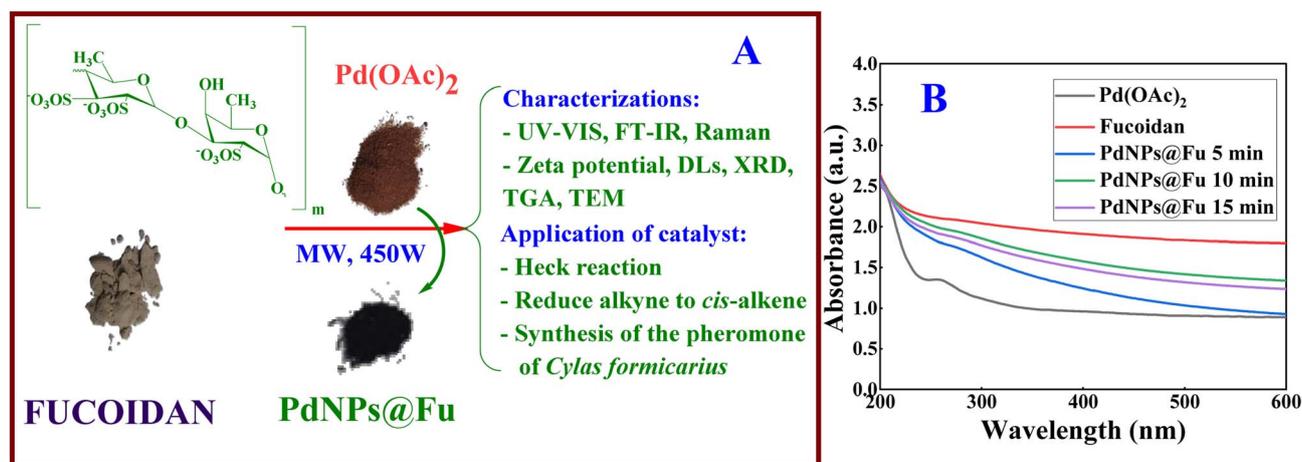

Fig. 1 (A) Diagrammatic depiction of the preparation of the catalyst and the application of PdNPs@Fu; and (B) UV-vis spectra of Pd(OAc)$_2$, PdNPs@Fu, and fucoidan.
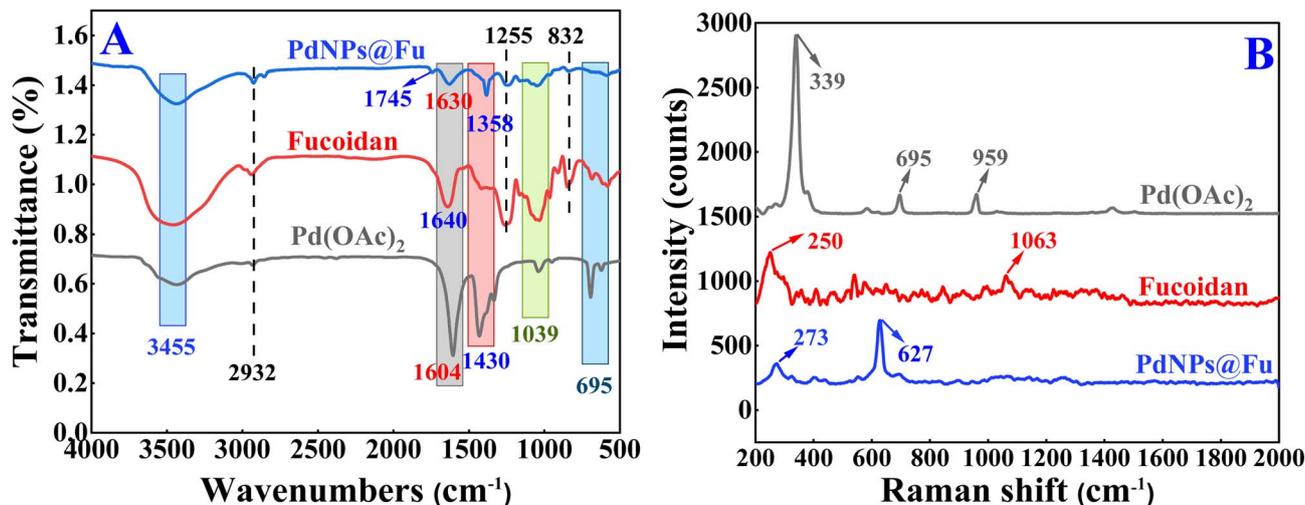
Fig. 2 (A) FT-IR spectra of PdNPs@Fu, Pd(OAc)$_2$, and fucoidan; (B) Raman spectra of PdNPs@Fu, Pd(OAc)$_2$, and fucoidan.

characteristic of the S=O stretching vibration, confirming the presence of sulfate esters in the fucoidan backbone. Additionally, the bands at around 1050 cm^{-1} are associated with C–O–C stretching and C–O bending vibrations of the sugar ring. In addition, upon the formation of the PdNPs@Fu nanocomposite, the S=O absorption band at 1255 cm^{-1} shifted to a lower wavenumber, accompanied by noticeable changes at 1039 and 832 cm^{-1}. A strong absorption band observed at 1745 cm^{-1} was attributed to the C=O stretching vibration of the ester (–COO–) groups derived from reducing sugars such as L-fucose, galactose, and glucose. These reducing moieties are likely generated from the partial hydrolysis of fucoidan and play a crucial role in the reduction of Pd^{2+} to Pd^0. Moreover, the disappearance or shifts of characteristic peaks corresponding to Pd(OAc)$_2$ confirmed the successful formation of Pd^0 nanoparticles. These spectral variations indicate the formation of stronger hydrogen bonds and coordination interactions between the –OH/SO$_3^-$ groups of fucoidan and the PdNPs@Fu surface. Therefore, fucoidan acts both as a bioreducing and a stabilizing agent for the PdNPs.[32–36]

Raman spectra were recorded using a 785 nm laser, with a 100 μm slit, a 100 μm confocal hole, a 25% optical filter, and a ×10 vis objective lens (Fig. 2B), the characteristic signals of

Pd(OAc)$_2$ at 339, 695, and 959 cm^{-1} completely disappeared upon the formation of the PdNPs@Fu catalyst, indicating the complete reduction of Pd^{2+} ions to metallic Pd^0. The appearance of new peaks at 273 and 627 cm^{-1} assigned to Pd–O vibrations and lattice modes associated with Pd–fucoidan interactions, further supports this transformation. Notably, the disappearance of the characteristic sulfate peak at 1063 cm^{-1} provides additional evidence for the involvement of –SO$_3^-$ groups in the coordination process during the formation of the PdNPs@Fu catalyst.[24,37–40]

Mechanistically, the FT-IR and Raman spectra reveal that the sulfate groups (–SO$_3^-$) in fucoidan act both as reducing and stabilizing agents for the PdNPs. The coordination between –SO$_3^-$ groups and Pd^{2+} ions facilitates the electron transfer and reduction of Pd^{2+} to Pd^0, while the highly negative surface charge induces strong electrostatic repulsion, preventing nanoparticle aggregation. In addition, the polysaccharide framework of fucoidan provides steric hindrance, further enhancing the colloidal stability of the system.[41–46]

The XRD pattern of PdNPs@Fu (Fig. 3A) exhibits four characteristic diffraction peaks at $2\theta = 40.2°, 46.5°, 68.4°$, and $82.1°$, which are indexed to the (111), (200), (220), and (311) crystal planes of face-centered cubic (fcc) metallic palladium (JCPDS
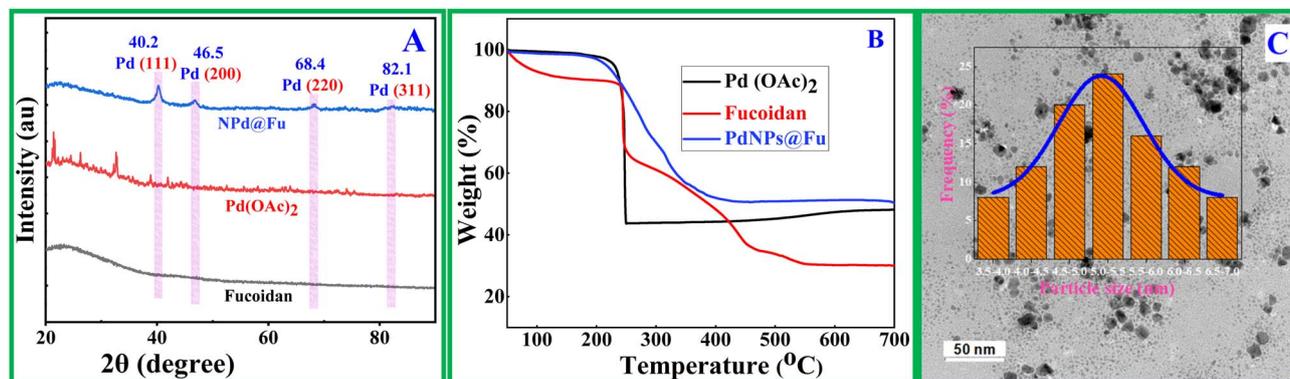

Fig. 3 XRD pattern (A) and TGA curves (B) of PdNPs@Fu, Pd(OAc)$_2$, fucoidan, and TEM (C) of PdNPs@Fu.

no. 46-1043), confirming the formation of PdNPs.[47,48] The absence of any additional peaks indicates that the PdNPs are highly phase-pure and well-crystallized. In contrast, no such reflections are observed in the XRD pattern of Pd(OAc)$_2$, confirming the complete reduction of Pd^{2+} ions to metallic Pd^0. The broadening of the diffraction peaks suggests the formation of Pd^0 crystals. These findings are in good agreement with previous reports, in which polysaccharide-mediated synthesis typically yields well-crystallized, small-sized PdNPs with narrow size distributions.[11,23,24]

The thermal stability of the PdNPs@Fu catalyst was evaluated *via* thermogravimetric analysis (TGA) under an airflow of 20 mL min^{-1} with a heating rate of 10 °C min^{-1} (Fig. 3B). During the initial stage (50–240 °C), Pd(OAc)$_2$, fucoidan, and PdNPs@Fu exhibited weight losses of 3%, 23%, and 2.4%, respectively, which are attributed to the loss of volatile components and adsorbed water.[49] The weight loss of the PdNPs@Fu composite was lower than that of Pd(OAc)$_2$ and fucoidan over the temperature range of 240–700 °C. Specifically, the weight losses of Pd(OAc)$_2$ and fucoidan were 53% and 35%, respectively, whereas PdNPs@Fu showed a 45% loss. Consequently, the residual ash of the nanocomposite (53%) is considerably higher than that of Pd(OAc)$_2$ (44%) and fucoidan (25%), which can be attributed to the presence of metallic palladium within the nanocomposite.

The TEM image clearly demonstrates the successful formation of PdNPs with small sizes, well-dispersed morphology, and minimal aggregation (Fig. 3C). The particle size distribution histogram reveals that most nanoparticles fall within the range of 2.0–6.0 nm, with an average size around 4.0 nm, indicating a narrow size distribution. Additionally, the particle size distribution of PdNPs@Fu was examined and fitted using a Gaussian model. The resulting histogram exhibited a narrow distribution, with an average particle size (x_C) of 3.83 ± 0.09 nm and a width (w) of approximately 2.23 nm. The high correlation between the Gaussian fitting and the experimental data (R^2 = 0.98; adjusted R^2 = 0.96) confirms the reliability and accuracy of the fitting model.[50–52] These observations indicate that the PdNPs@Fu nanoparticles are well-dispersed, possess uniform particle sizes, and show no evidence of aggregation.

These results indicate that employing fucoidan simultaneously as a bioreductant and stabilizing agent in an aqueous medium for the microwave-assisted synthesis of the PdNPs@Fu catalyst represents a highly effective strategy to produce nanomaterials with controllable particle size, enhanced dispersibility, and resistance to aggregation, while also exhibiting significant potential as a catalyst for organic transformations, particularly in pheromone synthesis. Fucoidan played a dual role during the synthesis process: the reducing sugars generated through partial hydrolysis act as electron donors for the reduction of Pd^{2+} to Pd^0, while its abundant hydroxyl and sulfate groups coordinate to the nanoparticle surface, providing effective stabilization. Moreover, the use of microwave irradiation at 450 W for 10 minutes provided rapid and uniform heating, accelerating the reduction process and promoting simultaneous nucleation, which resulted in the formation of ultrasmall and uniformly distributed nanoparticles.

The stability and particle size distribution of PdNPs@Fu nanocomposites in aqueous solution were evaluated using zeta potential (Fig. 4A–C) and dynamic light scattering (DLS)
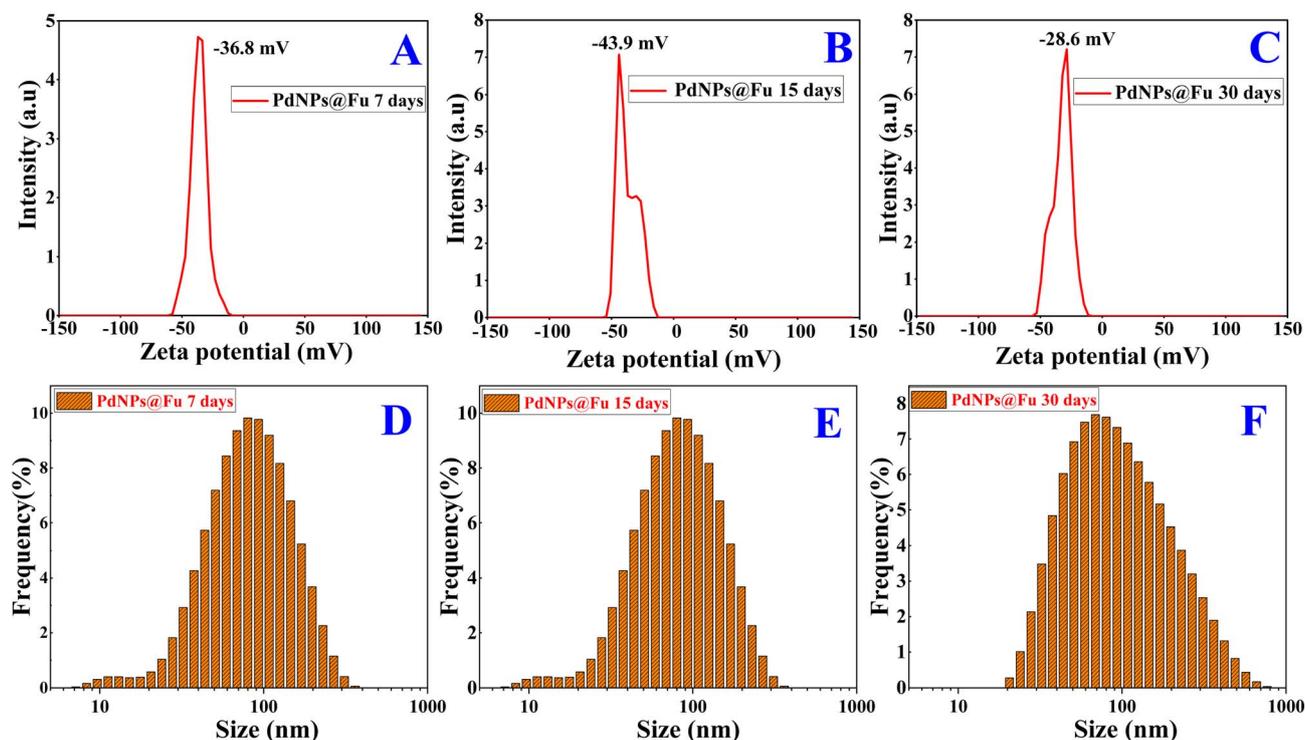

Fig. 4 Zeta potential (A–C) and dynamic light scattering (D–F) of PdNPs@Fu at different storage times (7, 15 and 30 days).

analysis at 25 °C (Fig. 4D–F). The experiments were conducted over a period of 30 days to monitor the temporal variation of the PdNPs@Fu colloidal system. During the first 7 days, the nanoparticles exhibited a zeta potential of −36.8 mV along with a narrow particle size distribution (40–200 nm), indicating relatively good colloidal stability. By day 15, the zeta potential became more negative, reaching −43.9 mV, while the particle size distribution remained narrow and uniform. The increase in the absolute value of zeta potential ($|\zeta|$) suggests a rise in surface charge density, which enhanced electrostatic repulsion between particles and resulted in an optimally stabilized colloidal state. This phenomenon can be attributed to the rearrangement of negatively charged functional groups ($-SO_3^-$, $-COO^-$) from fucoidan on the nanoparticle surface, increasing the surface charge density and improving surface coverage. However, by day 30, the zeta potential markedly decreased to −28.8 mV, accompanied by a clear shift in particle size distribution toward larger diameters (400–600 nm) with higher polydispersity. This observation reflects a reduction in surface charge-mediated stabilization and the onset of particle aggregation. Overall, the absolute magnitude of zeta potential exhibited an inverse relationship with particle growth: as $|\zeta|$ decreased, electrostatic repulsion weakened, promoting particle–particle collisions and aggregation.

Previous studies on other metallic nanoparticles have demonstrated similar observations. Venkatesan et al. (2018) reported that fucoidan–chitosan-coated silver nanoparticles (AgNPs) with highly negative zeta potential values exhibited prolonged colloidal stability, attributed to the strong electrostatic repulsion generated by the polysaccharide layer rich in sulfate and carboxyl groups.[11] Similarly, Souza et al. (2022) synthesized fucoidan-mediated AgNPs and observed that their zeta potential varied depending on environmental conditions, with phases of increased $|\zeta|$ corresponding to improved dispersion stability.[9] Furthermore, Chibowski et al. (2003) reported a non-linear variation of zeta potential in inorganic suspensions, characterized by an initial transient increase followed by a gradual decline, which was attributed to surface restructuring processes.[53]

The decline in zeta potential observed between days 15 and 30 can be rationalized based on the Derjaguin–Landau–Verwey–Overbeek (DLVO) theory, which describes the colloidal stability as a balance between electrostatic repulsion and van der Waals attraction. During the early stage (days 7–15), electrostatic repulsion predominates owing to the adsorption of negatively charged $-SO_3^-$ groups from fucoidan onto the surface of PdNPs, effectively preventing particle–particle collisions and aggregation. However, with prolonged storage, these functional groups tend to undergo surface rearrangement or become partially shielded as a result of polysaccharide chain interactions, leading to a reduction in surface charge density and consequently weakening the electrostatic stabilization of the colloidal system.[41–46]

This phenomenon was also reported by Chibowski et al. (2003) when investigating a $CaCO_3$ suspension system, in which the initial zeta potential increased and then gradually decreased

Table 1 Optimal investigation of Heck reaction for phenyl bromide and styrene[a]
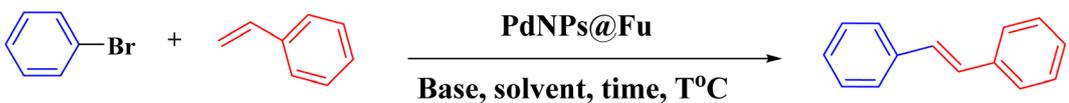
Entry	Base	Solvent	PdNPs@Fu (mg)	T^b (°C)	Time (h)	Yield[c]
1	K_2CO_3	DMF	0.5	90	4	62
2	K_2CO_3	DMF	1.0	90	4	74
3	K_2CO_3	DMF	2.0	90	6	80
4	K_2CO_3	DMF	3.0	90	6	78
5	K_2CO_3	DMF	1.0	100	4	85
6	**K_2CO_3**	**DMF**	**2.0**	**100**	**6**	**93**
7	K_2CO_3	DMF	3.0	100	6	88
8	K_2CO_3	DMF	2.0	110	6	86
9	K_2CO_3	DMF	3.0	110	6	84
10	Na_2CO_3	DMF	2.0	100	4	82
11	Na_2CO_3	DMF	2.0	100	6	86
12	Na_2CO_3	DMF	3.0	110	4	82
13	Na_2CO_3	DMF	3.0	110	6	80
14	K_2CO_3	DMSO	2.0	100	6	40
15	Na_2CO_3	DMSO	2.0	100	6	43
16	$(Et)_3N$	DMF	2.0	100	4	60
17	$(Et)_3N$	DMF	2.0	100	6	65
18	CH_3COONa	DMF	2.0	100	4	57
19	CH_3COONa	DMF	2.0	100	6	62
20	CH_3COONa	DMF	2.0	110	6	60

[a] Reaction conditions: phenyl bromide (1 mmol), styrene (2 mmol), base (1.2 mmol), solvent (2 mL). [b] Oil bath temperature. [c] Isolated yield.

over time due to surface restructuring.[53] Later, Pochapski et al. (2021) emphasized that the time-dependent variation of zeta potential is not an uncommon occurrence, but rather reflects surface kinetics and the equilibrium state of the electrical double layer influenced by the surrounding environment.[54] Therefore, the results obtained after 30 days for the PdNPs@Fu system are fully consistent with the phenomenon of time-dependent deterioration of surface charge stability, leading to nanoparticle aggregation and increased particle size important factor that should be carefully considered when designing storage conditions and practical applications.

Multidimensional experimental data establish that the microwave synthesis process is a green strategy optimally controlled by the synergistic mechanism for the synthesis of PdNPs@Fu. Fucoidan acts as both an electron source (via hydrolytic reduction) for the quantitative conversion of $Pd^{2+} \rightarrow Pd^0$, and establishes a stable electrosteric state by chemical adsorption of the surface sulfate group. The result is the formation of phase-pure (fcc), monodisperse Pd nanoparticles

at ultra-small size (3.83 ± 0.09 nm) and possessing outstanding thermal stability (53% residue), meeting the strict standards of modern nanocatalysis.

3.3. Catalytic performance for the Heck coupling

The catalytic performance of PdNPs@Fu was evaluated in the Heck coupling between various aryl bromide derivatives and styrene. The reaction was systematically optimized under different conditions, including temperature, solvent type, base, and functional substituents on the aryl bromides. Furthermore, the recyclability of the PdNPs@Fu catalyst was examined over five consecutive reaction cycles, and its surface characteristics were re-evaluated after reuse to verify the structural integrity and sustained catalytic efficiency.

The optimization (Table 1) showed that the highest yield of the Heck reaction (93%) was obtained when using 2 mg of the PdNPs@Fu catalyst, K_2CO_3 as the base, in DMF solvent at 100 °C for 6 hours (entry 6). When the catalyst amount was reduced below 2.0 mg, the yield dropped below 75%, whereas increasing

Table 2 Heck reaction of aryl halides and olefines

Entry	R_1	X	R_2	Time (h)	Yield[a]	TON	TOF (h^{-1})	Product
1	H	Cl	H	6	70	358	59.7	
2	H	Br	H	6	93	476	79.3	
3	H	I	H	6	94	481	80.2	**1a**
4	4-CH₃	Cl	4-OCH₃	6	68	348	58	
5	4-CH₃	Br	4-OCH₃	5	94	481	96.2	
6	4-CH₃	I	4-OCH₃	6	95	486	81.1	**1b**
7	4-CN	Cl	4-OCH₃	6	75	384	64	
8	4-CN	Br	4-OCH₃	5	95	486	97.3	
9	4-CN	I	4-OCH₃	4	96	491	122.9	**1c**
10	4-CH₃	Cl	4-F	6	63	323	53.8	
11	4-CH₃	Br	4-F	5	78	399	79.9	
12	4-CH₃	I	4-F	5	80	410	81.9	**1d**
13	4-CN	Cl	4-F	6	65	333	55.5	
14	4-CN	Br	4-F	6	79	404	67.4	
15	4-CN	I	4-F	6	83	425	70.8	**1e**
16	4-CH₃	Cl	4-Cl	6	55	282	46.9	
17	4-CH₃	Br	4-Cl	5	71	363	72.7	
18	4-CH₃	I	4-Cl	6	76	389	64.8	**1f**
18	4-CN	Cl	4-Cl	6	57	292	48.6	
20	4-CN	Br	4-Cl	6	78	399	66.6	
21	4-CN	I	4-Cl	5	85	435	87	**1g**

[a] Isolated yield.

it to 3.0 mg did not significantly improve the yield (around 88%), indicating that 2 mg is the optimal catalyst loading. Furthermore, at 90 °C, the reaction proceeded but with a yield below 80%; increasing the temperature to 100 °C afforded the highest yield (93%), while a further increase to 110 °C led to a slight decrease (86–88%), possibly due to catalyst decomposition or the occurrence of side reactions at elevated temperatures. Extending the reaction time from 4 to 6 hours markedly improved the yield to 93%, suggesting that 6 hours is the optimal reaction time for completion. The DMF solvent exhibited superior performance compared to DMSO. Being a polar aprotic solvent, DMF not only dissolves inorganic bases such as K_2CO_3 effectively but also stabilizes the reaction intermediates and facilitates C–Br bond activation, thereby affording higher yields, a trend consistent with previous studies.[55,56] In contrast, DMSO, due to its strong coordinating ability toward Pd, reduces the catalytic activity, resulting in lower yields (40–43%). The use of K_2CO_3 gave the best results owing to its moderate basicity, which is suitable for the deprotonation and Pd^0 regeneration steps. On the other hand, Na_2CO_3 and CH_3-COONa, with weaker basicity, afforded moderate yields (57–86%), while $(Et)_3N$, although an organic base, did not favor the stabilization of reaction intermediates, leading to moderate yields (60–65%). Notably, in this case, the Heck reaction proceeded efficiently without the assistance of any ligands such as PPh_3,[57] L·HBr (L = (1-ethylenediphenylphosphino-3-(mesityl)) imidazol-2-ylidene),[58] triaryl phosphine-functionalized imidazolium salts.[59]

Table 2 summarizes the synthesis of compounds **1a–1g**, revealing that the Heck coupling efficiency strongly depends on the nature of the halide (X) and the substituents (R_1, R_2) on the aryl or olefin moiety. Aryl iodides afforded the highest yields (94–96%, entries 3, 6 and 9), followed by bromides (93–95%, entries 2, 5, 8, 13, 16 and 20), whereas chlorides showed markedly lower activity (63–70%, entries 1, 4, 7, 10, 14 and 17). This trend agrees well with previous reports, as the weaker C–I bond facilitates oxidative addition to Pd^0 more readily than the stronger C–Cl bond. The electronic effects of substituents (R_1) on the aromatic ring also played a decisive role. Electron-donating groups (EDGs) such as –CH_3 and –OCH_3 enhanced the yields (94–96%, entries 5, 6 and 9), while electron-

withdrawing groups (EWGs) like –CN reduced them (65–85%, entries 7, 8, 9, 13, 15, 19 and 21). This can be rationalized by the Hammett correlation: EDGs ($\sigma < 0$) increase the electron density on the aromatic ring, facilitating Pd insertion and stabilizing intermediates, whereas EWGs ($\sigma > 0$) withdraw electron density and suppress catalytic activity.[60,61] Similarly, for the olefin component, substrates bearing electron-donating substituents (–OCH_3, –CH_3) on the aryl ring gave superior yields (94–96%, entries 5, 6 and 9), while those containing electron-withdrawing groups (–F, –Cl) resulted in significantly lower yields (63–83%, entries 10–17). This observation aligns with the reaction mechanism, where electron-rich olefins enhance the rate of Pd–C insertion, while electron-deficient olefins exhibit diminished reactivity. Overall, the reactivity trend follows the order I > Br > Cl, and electron-donating substituents ($\sigma < 0$) generally afford higher yields than electron-withdrawing ones ($\sigma > 0$) on both the aryl and olefin partners.[56]

The catalysis recycle results were presented in Fig. 5. After five catalytic cycles, an isolated yield of approximately 94% was maintained. TEM analysis revealed that while the particle size remained stable at 4–4.5 nm, the morphology of the catalyst particles gradually transformed from polyhedral to spherical (Fig. 5B). Moreover, the particle size distribution of PdNPs@Fu modeled using a Gaussian function displays a narrow distribution, with an average particle diameter (x_C) of 5.14 ± 0.14 nm and a width (w) of approximately 2.21 nm. The excellent correlation between the Gaussian fit and experimental data ($R^2 = 0.94$, adjusted $R^2 = 0.90$) confirms the accuracy of the model. These results indicate that the PdNPs@Fu nanoparticles are uniformly dispersed with a consistent particle size. The findings verify that the adopted synthesis successfully produced PdNPs with a homogeneous and stable distribution, highlighting the robustness and catalytic potential of PdNPs@Fu for Heck reduction.

The XRD analysis shows that before the reaction (Fig. 3A), the characteristic diffraction peaks corresponding to Pd (111), Pd (200), Pd (220), and Pd (311) are clearly visible, confirming the well-defined crystalline nature of the nanopalladium catalyst. Following the Heck catalytic process (Fig. 5C), these peaks are still observed; however, slight shifts in peak positions and minor variations in intensity appear. Such changes suggest subtle
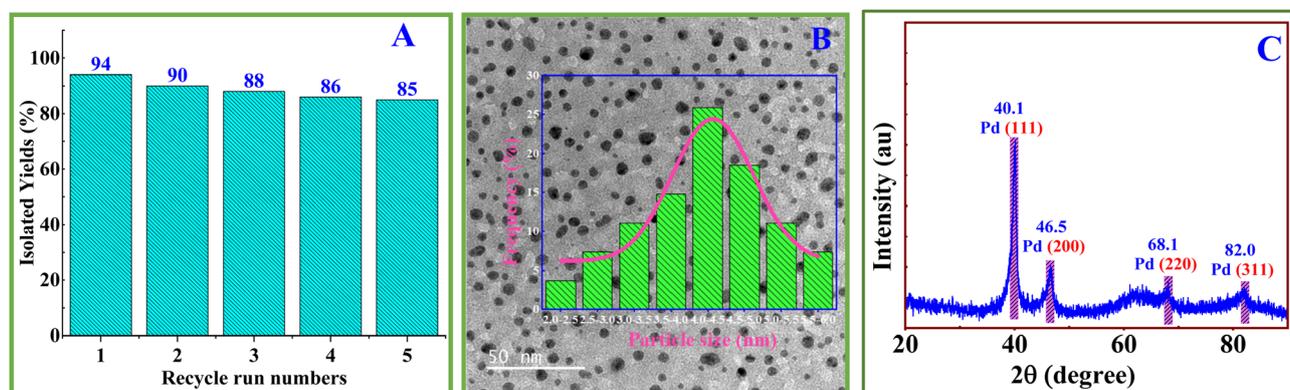

Fig. 5 Recyclable catalysis performance of PdNPs@Fu for Heck coupling between iodobenzene and styrene (A); TEM, size distribution (B), and XRD (C) analyses of PdNPs@Fu after five Heck catalytic runs.

structural perturbations of the PdNPs due to interactions with the reagents during the coupling reaction. This modification can be attributed to changes in the surface structure and lattice strain of the Pd particles resulting from the catalytic cycle.

This transformation suggests that the reaction did not proceed through a pronounced Ostwald ripening process. Instead, the phenomenon can be attributed to the surface atom rearrangement occurring during catalysis, whereby high-energy atoms located at edges and corners migrate to more stable positions. Consequently, the particles tend to adopt a spherical geometry to minimize surface energy, without inducing a significant change in overall particle size.[62] In a comparative evaluation, the PdNPs@Fu nanocomposite exhibited catalytic activity comparable to other reported catalyst systems for the Heck coupling reaction in DMF without the need for any phosphine ligand (PPh₃). These findings indicate that the PdNPs@Fu nanocomposite represents a promising material for C–C coupling catalysis.

3.4. Catalytic performance for the reduction of alkynes

Table 3 summarizes the outcomes of the hydrogenation of alkynes 2a–2e catalyzed by PdNPs@Fu, in which DMF served both as solvent and hydrogen donor under various conditions. Aryl-substituted alkynes afforded high yields (93–95%, entries 1–4), indicating the strong catalytic activity of PdNPs@Fu toward aromatic substrates. In contrast, aliphatic alkynes bearing the –CH₂OTHP group provided slightly lower but still high yields (85–94%, entries 5–7). This result highlights the necessity of OTHP protection to prevent catalyst poisoning by free hydroxyl groups; in the absence of such protection, only a trace yield was obtained (entry 12), consistent with previous reports.[63]

The optimal reaction conditions were determined as 2.0 mg PdNPs@Fu, 110 °C for 6 h (entry 7). In comparison, previous studies employing traditional Pd catalysts such as Pd(OAc)₂, PdCl₂, Pd(PPh₃)₂Cl₂, Pd₂(dba)₃, or nanostructured systems such

as PdNPs@pectin and PdNPs@β-CD–CMC for the conversion of alkynes to cis-alkenes typically required 1–5 mol% of catalyst relative to the substrate.[23,24,63,64] These findings demonstrate that PdNPs@Fu not only improve the efficiency of the reduction but also reduce the consumption of precious metals while maintaining the possibility of reusability. However, increasing the catalyst loading to 3.0 mg did not lead to any significant improvement in yield (entry 8). Furthermore, the choice of base had a clear impact on the reaction efficiency, likely by promoting DMF hydrolysis. In this study, NaOH and K₂CO₃ afforded only moderate yields, while KOH provided superior results (entries 9 and 10).
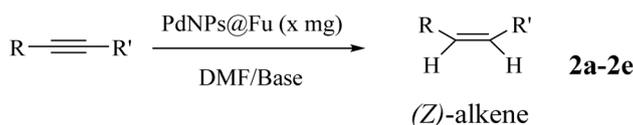
In short, PdNPs@Fu demonstrated outstanding efficiency and remarkable chemoselectivity in the transformation of alkynes into (Z)-alkenes. This highlights its great potential as a promising catalytic system for alkyne-to-(Z)-alkene reductions and for various applications, particularly in the synthesis of (Z)-alkene pheromones, thereby contributing to the advancement of high-tech agriculture.

The recycle results are shown in Fig. 6A. An isolated yield of approximately 85% was achieved after five consecutive recycling cycles. TEM analysis revealed that while the particle size remained stable at 4–5 nm, the morphology of the catalyst particles gradually transformed from polyhedral to spherical (Fig. 6B). This transformation suggests that the reaction did not proceed through a pronounced Ostwald ripening process. Instead, the phenomenon can be attributed to the surface atom rearrangement occurring during catalysis, whereby high-energy atoms located at edges and corners migrate to more stable positions.[65–68] Consequently, the particles tend to adopt a spherical geometry to minimize surface energy, without inducing a significant change in overall particle size, similar to the Heck reaction.[62] Furthermore, the particle size distribution of PdNPs@Fu was analyzed and fitted using a Gaussian model. The

Table 3 Reaction conditions for alkyne reaction in the presence of PdNPs@Fu

$$ R\!\!=\!\!\!=\!\!R' \xrightarrow[\text{DMF/Base}]{\text{PdNPs@Fu (x mg)}} \underset{H \quad \quad H}{R\!\!=\!\!\!=\!\!R'} \quad \textbf{2a-2e} $$

(Z)-alkene

Entry	R	R′	Time (h)	PdNPs@Fu (mg)	Temp.[a] (°C)	Base	Isolated yield	TON	TOF (h⁻¹)
1	C₆H₅–	H	6	2.0	110	KOH	95 (2a)	486	81.1
2	4-Cl–C₆H₄–	H	6	2.0	110	KOH	94 (2b)	481	80.2
3	C₆H₅–	C₆H₅–	6	2.0	110	KOH	94 (2c)	481	80.2
4	3-OCH₃–C₆H₄–	C₆H₅–	6	2.0	110	KOH	93 (2d)	476	79.3
5	CH₃–	–CH₂–OTHP	6	2.0	100	KOH	90 (2e)	461	76.8
6	CH₃–	–CH₂–OTHP	6	1.0	110	KOH	85 (2e)	870	145
7	**CH₃–**	**–CH₂–OTHP**	**6**	**2.0**	**110**	**KOH**	**94 (2e)**	**481**	**80.2**
8	CH₃–	–CH₂–OTHP	6	3.0	120	KOH	93 (2e)	317	52.9
9	CH₃–	–CH₂–OTHP	6	2.0	110	K₂CO₃	72 (2e)	369	61.4
10	CH₃–	–CH₂–OTHP	6	2.0	110	NaOH	65 (2e)	333	55.5
11	CH₃–	–CH₂–OTHP	8	0.0	120	KOH	0	0	0
12	CH₃–	–CH₂–OH	6	2.0	120	KOH	Trace	Trace	Trace

[a] Oil bath temperature, THP: 2-tetrahydropyranyl.

Fig. 6 Recyclable catalysis performance of PdNPs@Fu for 2-(but-2-yn-1-yloxy)tetrahydro-2H-pyran reduction (A); TEM image, size distribution (B), XRD (C) analyses of PdNPs@Fu for alkyne reduction after five catalytic runs, and the signals of the two protons at the double bond of 2-(but-3-en-1-yloxy)tetrahydro-2H-pyran (D) (**2e**).

histogram results reveal a narrow distribution with an average particle size (x_C) of approximately 4.17 ± 0.09 nm and a width (w) of about 2.23 nm. The R-square value of 0.98, along with an adjusted R-square of 0.96, indicates that the Gaussian fitting is highly consistent with the experimental data. This confirms that PdNPs@Fu nanoparticles exhibit a uniform size distribution and good dispersion. These results demonstrate that the synthetic procedure successfully produced Pd nanoparticles with a homogeneous and stable size distribution. Taken together, these findings highlight the PdNPs@Fu nanocomposite as a highly robust and promising material for alkyne reduction.

After the catalytic process (Fig. 6C), the characteristic reflections of Pd, including Pd (111), Pd (200), Pd (220), and Pd (311), remain detectable, confirming that the crystalline framework of the metallic phase is largely preserved. Nevertheless, slight shifts in peak positions together with a discernible broadening are observed. Such evolution in the diffraction profile typically reflects changes in crystallite size, lattice strain, or particle dispersion. These alterations likely originate from the interaction of Pd with the alkyne substrate during its conversion to the corresponding cis-alkene, which can induce partial surface reconstruction or subtle changes in nanoparticle dimensions. Thus, the post-reaction XRD patterns suggest that although the Pd core remains intact, the catalytic cycle exerts a measurable influence on the surface characteristics of the nanoparticles.

On the ^1H NMR spectrum of compound (**2e**), the characteristic proton signals of the tetrahydropyranyl protecting group were observed at δ 4.65–4.63 ppm (m, 1H, –OCHO), 4.29–3.82 ppm (m, 2H, –CH$_2$O–), and 3.54–3.50 ppm (m, 2H, –CH$_2$-OTHP). Additionally, the vinyl protons (–CH= and =CH–)

appeared at δ 5.69–5.64 ppm (dtt, J = 10.8, 6.0, 1.8 Hz, 1H) and 5.61–5.56 ppm (dtt, J = 10.8, 7.2, 1.2 Hz, 1H), confirming the formation of 2-(but-3-en-1-yloxy)tetrahydro-2H-pyran (**2e**). Furthermore, the coupling constant (J < 12 Hz) was consistent with the (Z)-configuration of compound (**2e**)[24] (Fig. 6C).

Kinetic and quantitative analysis confirmed that PdNPs@Fu possesses superior intrinsic efficiency due to its ultra-small particle structure (~3.8 nm) and high metal loading (10.39% wt), maximizing surface area/volume ratio and low-coordinate sites. For the Heck reaction mechanism, the activity closely follows the oxidative addition (RDS) kinetics, with a priority order of I > Br > Cl, and is promoted by electron-withdrawing groups (EWGs) that lower the antibonding σ^* orbital energy. The ability to efficiently activate the inert C–Cl bond demonstrates the optimal electron density at the Pd^0 center.

Moreover, in alkyne semi-hydrogenation kinetics, the catalyst exhibits a practical activity potential up to TOF 145 h^{-1} (when minimizing the diffusion limit/kinetic excess), operating efficiently by the transfer hydrogenation mechanism. However, the system is susceptible to catalyst poisoning by free hydroxyl groups through competitive adsorption/surface chelation. Thus, the role of Fucoidan is not only to stabilize the particle size but also to modulate the ideal electron density for the Pd^0/Pd^{2+} catalytic cycle, creating a stable and high-performance heterogeneous catalyst system.

3.5. Application of PdNPs@Fu catalyst for the synthesis of insect pheromone

Cylas formicarius, a species of sweet potato weevil belonging to the family Brentidae, is broadly distributed worldwide. Its sex

Scheme 1 Synthesis of *Cylas formicarius* pheromone.
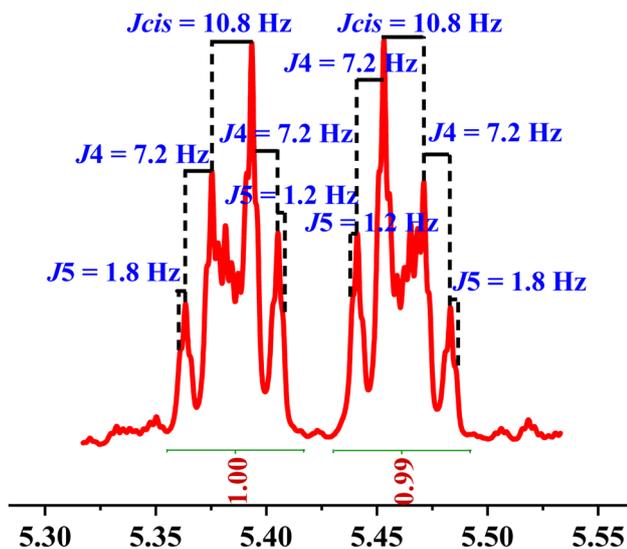
Fig. 7 Compound (**4**) exhibited two sets of (*Z*)-alkene signal protons at δ_H 5.41–5.36 ppm and δ_H 5.45–5.44 ppm.

pheromone has been identified as (*Z*)-3-dodecen-1-yl (*E*)-2-butenoate.[69,70] The synthetic pathway is outlined in Scheme 1. The first key step involved a coupling between 1-decyne and 2-((2-bromoethanyl)oxy)tetrahydro-2*H*-pyran (**2**), affording the alkyne derivative (**3**). Subsequent reduction of (**3**) using KOH/DMF in the presence of PdNPs@Fu at 110 °C provided compound (**4**) in 92% yield. Removal of the protecting group then furnished (*Z*)-3-dodecen-1-ol (**5**) with 91% yield. Esterification of (**5**) with crotonyl chloride in pyridine produced the pheromone (**6**) in 94% yield. The ^{1}H NMR spectrum of compound (**4**) displayed a coupling constant of 10.5–11.0 Hz for the vinyl protons, confirming the *cis*-configuration of the synthesized alkene. The overall yield for the pheromone synthesis was approximately 78%.

The pivotal intermediate in the pheromone synthesis is compound (**4**). Structural analysis of (**4**) revealed that the NMR spectral data were consistent with previous reports.[2,4,5,11] In the ^{1}H NMR spectrum, a pair of double signals corresponding to olefinic protons was observed at δ 5.41–5.36 ppm (dtt, J = 10.8, 7.2, 1.2 Hz, 1H) and δ 5.45–5.44 ppm (dtt, J = 10.8, 7.2, 1.8 Hz). The coupling constant (J < 12 Hz) confirmed the (*Z*)-configuration of the main carbon chain (Fig. 7).

4   Conclusions

In this study, we successfully developed a green and efficient microwave-assisted method for the synthesis of PdNPs using fucoidan as both a bioreductant and stabilizing agent in an aqueous medium. The resulting nanoparticles exhibited an average size of approximately 4 nm and excellent colloidal stability for up to 15 days at room temperature. The catalytic performance of PdNPs@Fu was demonstrated in the Heck coupling reaction, achieving a yield of 93% and maintaining high activity after five consecutive reuse cycles. Similarly, the catalyst exhibited outstanding activity in the selective semi-hydrogenation of alkynes to (*Z*)-alkenes, affording a 94% yield

and retaining 85% efficiency after five recycles, indicating excellent durability and reusability. Furthermore, the catalytic system showed promising potential in the synthesis of the sweet potato weevil (*Cylas formicarius*) pheromone, with an overall yield of 78%. Taken together, the use of fucoidan as a sustainable biogenic agent enables a green synthetic route toward highly stable and recyclable PdNPs@Fu nanocatalysts. These findings not only advance the field of environmentally benign catalysis but also open promising avenues for sustainable applications in pharmaceuticals, medicine, and agriculture.

Author contributions

Van-Dung Le, Minh-Vuong Phan: conceptualization, methodology, supervision, validation, and writing – review; Nhat-Minh Phan, Nguyen-Khanh-Vu Ngo, Thi-Yen-Nghi Le, Truc-Vy Mai, Duc-Huy Pham, Minh-Trong Tran, Minh-Ty-Nguyen, Thi-Cam-Thu Nguyen, Thanh-Danh Nguyen, Dinh-Tri Mai, Thi-Ngoc Mai Tran, Thi-Thanh-Tu Nguyen, Hoang-Nhu-Khanh Huynh: data curation, formal analysis, methodology, validation, visualization; Chi-Hien Dang: funding acquisition, methodology, project administration, resources, supervision, and writing – review & editing.

Conflicts of interest

No potential conflict of interest was reported by the authors.

Data availability

All data needed to support the conclusions of this paper are fully presented in the paper and supporting information (SI). Supplementary information: detailed experimental procedures for the Heck coupling reaction, alkyne reduction, and the synthesis of insect pheromone. Additional data, including GC-MS, ^{1}H NMR, and ^{13}C NMR analyses. See DOI: https://doi.org/10.1039/d5ra08010j.

Acknowledgements

References

1 C. O. Kappe, Controlled microwave heating in modern organic synthesis, *Angew. Chem., Int. Ed.*, 2004, **43**, 6250–6284.

2 V. Polshettiwar and R. S. Varma, Microwave-assisted organic synthesis and transformations using benign reaction media, *Acc. Chem. Res.*, 2008, **41**, 629–639.

3 F. Geinguenaud, O. Sainte-Catherine, F. Poirier, V. Besnard, O. Haddad, F. Chaubet, *et al.*, Iron oxide nanoparticles functionalized with fucoidan: a potential theranostic nanotool for hepatocellular carcinoma, *ChemBioChem*, 2022, **23**, e202200265.

© 2025 The Author(s). Published by the Royal Society of Chemistry

4 C.-S. Chiang, B.-J. Huang, J.-Y. Chen, W. W. Chieng, S. H. Lim, W. Lee, *et al.*, Fucoidan-based nanoparticles with inherently therapeutic efficacy for cancer treatment, *Pharmaceutics*, 2021, **13**, 1986.

5 A. S. E. Newehy, S. F. Gheda, M. M. Ismail, D. Aldisi, M. M. Abulmeaty and M. E. Elshobary, Fucoidan-Based Gold Nanoparticles: Antioxidant and Anticancer Potential from Turbinaria decurrens and Sargassum cinereum, *Pharmaceutics*, 2025, **17**, 826.

6 J. Dupont, C. S. Consorti and J. Spencer, The potential of palladacycles: more than just precatalysts, *Chem. Rev.*, 2005, **105**, 2527–2572.

7 D. Astruc, Palladium nanoparticles as efficient green homogeneous and heterogeneous carbon–carbon coupling precatalysts: a unifying view, *Inorg. Chem.*, 2007, **46**, 1884–1894.

8 Z. Han, L. Dong, J. Zhang, T. Cui, S. Chen, G. Ma, *et al.*, Green synthesis of palladium nanoparticles using lentinan for catalytic activity and biological applications, *RSC Adv.*, 2019, **9**, 38265–38270.

9 A. O. Souza, J. W. d. F. Oliveira, C. J. G. Moreno, M. J. C. de Medeiros, M. M. Fernandes-Negreiros, F. R. M. Souza, *et al.*, Silver nanoparticles containing fucoidan synthesized by green method have anti-Trypanosoma cruzi activity, *Nanomaterials*, 2022, **12**, 2059.

10 S. S. Rao, K. Saptami, J. Venkatesan and P. Rekha, Microwave-assisted rapid synthesis of silver nanoparticles using fucoidan: characterization with assessment of biocompatibility and antimicrobial activity, *Int. J. Biol. Macromol.*, 2020, **163**, 745–755.

11 J. Venkatesan, S. K. Singh, S. Anil, S.-K. Kim and M. S. Shim, Preparation, characterization and biological applications of biosynthesized silver nanoparticles with chitosan-fucoidan coating, *Molecules*, 2018, **23**, 1429.

12 S. Rajeshkumar, E. Aboelfetoh, S. Balusamy, D. Ali, M. Almarzoug, J. Tesfaye, *et al.*, Anticancer, enhanced antibacterial, and free radical scavenging potential of fucoidan-(Fucus vesiculosus Source) mediated silver nanoparticles, *Oxid. Med. Cell. Longev.*, 2021, **2021**, 8511576.

13 S. M. Lim, K. Kang, H. Jang and J. T. Park, Environmental friendly synthesis of hierarchical mesoporous platinum nanoparticles templated by fucoidan biopolymer for enhanced hydrogen evolution reaction, *J. Mater. Sci. Technol.*, 2020, **46**, 185–190.

14 P.-A. Hwang, X.-Z. Lin, K.-L. Kuo and F.-Y. Hsu, Fabrication and cytotoxicity of fucoidan-cisplatin nanoparticles for macrophage and tumor cells, *Materials*, 2017, **10**, 291.

15 J. Goncalves, C. Nunes, L. Ferreira, M. M. Cruz, H. Oliveira, V. Bastos, *et al.*, Coating of magnetite nanoparticles with fucoidan to enhance magnetic hyperthermia efficiency, *Nanomaterials*, 2021, **11**, 2939.

16 J. Matusiak, E. Grządka, A. Bastrzyk and S. Pasieczna-Patkowska, The influence of fucoidan on stability, adsorption and electrokinetic properties of ZnO and TiO2 suspensions, *Appl. Nanosci.*, 2022, **12**, 919–927.

17 N. Joudeh, A. Saragliadis, G. Koster, P. Mikheenko and D. Linke, Synthesis methods and applications of palladium nanoparticles: a review, *Front. Nanotechnol.*, 2022, **4**, 1062608.

18 M. Alinaghi, P. Mokarram, M. Ahmadi and F. Bozorg-Ghalati, Biosynthesis of palladium, platinum, and their bimetallic nanoparticles using rosemary and ginseng herbal plants: evaluation of anticancer activity, *Sci. Rep.*, 2024, **14**, 5798.

19 S. Choudhary, G. Kumawat, K. Kher, P. Baroliya, A. K. Gupta and M. K. Tripathy, Green synthesis of palladium nanoparticles using Asterarcys sp. and their applications, *Nano TransMed*, 2024, **3**, 100046.

20 S. Bi and R. Srivastava, Bottom-up synthesis of palladium nanoparticles: kinetics effect and catalytic activity, *Polyhedron*, 2025, **269**, 117426.

21 S. Vinodhini, B. S. M. Vithiya and T. A. A. Prasad, Green synthesis of palladium nanoparticles using aqueous plant extracts and its biomedical applications, *J. King Saud Univ., Sci.*, 2022, **34**, 102017.

22 R. K. Borah, A. Mahanta, A. Dutta, U. Bora and A. J. Thakur, A green synthesis of palladium nanoparticles by Sapindus mukorossi seed extract and use in efficient room temperature Suzuki–Miyaura cross-coupling reaction, *Appl. Organomet. Chem.*, 2017, **31**, e3784.

23 V.-D. Le, T. C.-H. Le, V.-T. Chau, T. N.-D. Le, C.-H. Dang, T. T.-N. Vo, *et al.*, Palladium nanoparticles in situ synthesized on Cyclea barbata pectin as a heterogeneous catalyst for Heck coupling in water, the reduction of nitrophenols and alkynes, *New J. Chem.*, 2021, **45**, 4746–4755.

24 V.-D. Le, T. K. C. Huynh, C.-H. Dang and T. Y. N. Le, Palladium nanoparticles from β-cyclodextrin and cellulose methyl carboxylate as an effective catalyst for Sonogashira coupling and the reduction of alkynes, *RSC Adv.*, 2025, **15**, 10534–10546.

25 X. Zhao, Y. Chang, W.-J. Chen, Q. Wu, X. Pan, K. Chen, *et al.*, Recent progress in Pd-based nanocatalysts for selective hydrogenation, *ACS Omega*, 2021, **7**, 17–31.

26 J. Ballesteros-Soberanas, J. A. Carrasco and A. Leyva-Pérez, Parts-per-million of soluble Pd0 catalyze the semi-hydrogenation reaction of alkynes to alkenes, *J. Org. Chem.*, 2022, **88**, 18–26.

27 J. Shi, T. Ye, J. Dong, A. Liu, T. Xu, M. Tai, *et al.*, H2O as the Hydrogen Donor: Stereo-Selective Synthesis of E-and Z-Alkenes by Palladium-Catalyzed Semihydrogenation of Alkynes, *ACS Omega*, 2023, **8**, 11492–11502.

28 V. L. Silva and A. M. Silva, Palladium-catalysed synthesis and transformation of quinolones, *Molecules*, 2019, **24**, 228.

29 M. B. Gawande, A. Goswami, T. Asefa, H. Guo, A. V. Biradar, D.-L. Peng, *et al.*, Core–shell nanoparticles: synthesis and applications in catalysis and electrocatalysis, *Chem. Soc. Rev.*, 2015, **44**, 7540–7590.

30 F. Yousefnejad, S. Bahadorikhalili, M. Esmkhani, M. Adib, S. Javanshir, S. Hosseini, *et al.*, Palladium supported magnetic fucus vesiculosus extract as a natural and novel catalyst for the synthesis of N-alkyl-2-(4-methyl-1-oxoisoquinolin-2 (1 H)-yl)-2-phenylacetamide derivatives, *Sci. Rep.*, 2023, **13**, 1272.

31 S. Wunder, F. Polzer, Y. Lu, Y. Mei and M. Ballauff, Kinetic analysis of catalytic reduction of 4-nitrophenol by metallic nanoparticles immobilized in spherical polyelectrolyte brushes, *J. Phys. Chem. C*, 2010, **114**, 8814–8820.

32 P. Lin, S. Chen, M. Liao and W. Wang, Physicochemical characterization of fucoidans from Sargassum henslowianum C. Agardh and their antithrombotic activity in vitro, *Mar. Drugs*, 2022, **20**, 300.

33 M. R. Soto-Vásquez, P. A. A. Alvarado-García, F. S. Youssef, M. L. Ashour, H. A. Bogari and S. S. Elhady, FTIR characterization of sulfated polysaccharides obtained from Macrocystis integrifolia algae and verification of their antiangiogenic and immunomodulatory potency in vitro and in vivo, *Mar. Drugs*, 2022, **21**, 36.

34 A. Zayed, K. Muffler, T. Hahn, S. Rupp, D. Finkelmeier, A. Burger-Kentischer, *et al.*, Physicochemical and biological characterization of fucoidan from Fucus vesiculosus purified by dye affinity chromatography, *Mar. Drugs*, 2016, **14**, 79.

35 J. Chale-Dzul, R. Moo-Puc, D. Robledo and Y. Freile-Pelegrín, Hepatoprotective effect of the fucoidan from the brown seaweed Turbinaria tricostata, *J. Appl. Phycol.*, 2015, **27**, 2123–2135.

36 J. Chale-Dzul, R. Moo-Puc, D. Robledo and Y. Freile-Pelegrín, Hepatoprotective effect of the fucoidan from the brown seaweed, *5th Congress of the International Society for Applied Phycology*, 2014, vol. 27, pp. 2123–2135.

37 S. H. Ptak, L. Sanchez, X. Fretté and D. Kurouski, Complementarity of Raman and Infrared spectroscopy for rapid characterization of fucoidan extracts, *Plant Methods*, 2021, **17**, 130.

38 M. Zhao, M. Garcia-Vaquero, J. Przyborska, S. P. Sivagnanam and B. Tiwari, The development of analytical methods for the purity determination of fucoidan extracted from brown seaweed species, *Int. J. Biol. Macromol.*, 2021, **173**, 90–98.

39 H. Jang, K. Kang and M. A. El-Sayed, Real-time tracking of the autophagy process in living cells using plasmonically enhanced Raman spectroscopy of fucoidan-coated gold nanoparticles, *J. Mater. Chem. B*, 2018, **6**, 5460–5465.

40 S. Jeong, S. Lee, G. Lee, J. Hyun and B. Ryu, Systematic characteristics of fucoidan: intriguing features for new pharmacological interventions, *Int. J. Mol. Sci.*, 2024, **25**, 11771.

41 B. Derjaguin, N. Churaev and V. Muller, The Derjaguin–Landau–Verwey–Overbeek (DLVO) theory of stability of lyophobic colloids, in *Surface Forces*, Springer, 1987, pp. 293–310.

42 D. Saha, R. Bandyopadhyay and Y. M. Joshi, Dynamic light scattering study and DLVO analysis of physicochemical interactions in colloidal suspensions of charged disks, *Langmuir*, 2015, **31**, 3012–3020.

43 R. Daneshfar, S. Ashoori and B. S. Soulgani, Interaction of electrolyzed nanomaterials with sandstone and carbonate rock: experimental study and DLVO theory approach, *Geoenergy Sci. Eng.*, 2023, **230**, 212218.

44 D. Takács, T. Péter, Z. V. Árok, B. Katana, S. Papović, S. Gadzuric, *et al.*, Structure–Stability Relationship in Aqueous Colloids of Latex Particles and Gemini Surfactants, *J. Phys. Chem. B*, 2022, **126**, 9095–9104.

45 A. Serrano-Lotina, R. Portela, P. Baeza, V. Alcolea-Rodríguez, M. Villarroel and P. Ávila, Zeta potential as a tool for functional materials development, *Catal. Today*, 2023, **423**, 113862.

46 L. Spitzmüller, J. Berson, T. Kohl, T. Schimmel and F. Nitschke, Design of silica nanoparticle tracers with optimized dispersion stability, sorption and deposition properties based on (X) DLVO and filtration theory, *Geothermics*, 2025, **130**, 103309.

47 K. Walbrück, F. Kuellmer, S. Witzleben and K. Guenther, Synthesis and Characterization of PVP-Stabilized Palladium Nanoparticles by XRD, SAXS, SP-ICP-MS, and SEM, *J. Nanomater.*, 2019, **2019**, 4758108.

48 A. J. Kora and L. Rastogi, Green synthesis of palladium nanoparticles using gum ghatti (Anogeissus latifolia) and its application as an antioxidant and catalyst, *Arab. J. Chem.*, 2018, **11**, 1097–1106.

49 A. Nuri, N. Vucetic, J.-H. Smått, Y. Mansoori, J.-P. Mikkola and D. Y. Murzin, Synthesis and characterization of palladium supported amino functionalized magnetic-MOF-MIL-101 as an efficient and recoverable catalyst for Mizoroki–Heck cross-coupling, *Catal. Lett.*, 2020, **150**, 2617–2629.

50 W. Zhou, C. Ma, T. Yao, P. Chang, Q. Zhang and A. Kuijper, Histograms of Gaussian normal distribution for 3D feature matching in cluttered scenes, *Vis. Comput.*, 2019, **35**, 489–505.

51 D. Mukherjee, L. Miao, G. Stone and N. Alem, mpfit: a robust method for fitting atomic resolution images with multiple Gaussian peaks, *Adv. Struct. Chem. Imaging*, 2020, **6**, 1.

52 M. Debangshu, M. Leixin, G. Stone and A. Nasim, mpfit: a robust method for fitting atomic resolution images with multiple Gaussian peaks, *Adv. Struct. Chem. Imaging*, 2020, **6**, DOI: 10.1186/s40679-020-0068-y.

53 E. Chibowski, L. Hotysz and A. Szcześ, Time dependent changes in zeta potential of freshly precipitated calcium carbonate, *Colloids Surf., A*, 2003, **222**, 41–54.

54 D. J. Pochapski, C. C. dos Santos, G. W. Leite, S. H. Pulcinelli and C. V. Santilli, Zeta potential and colloidal stability predictions for inorganic nanoparticle dispersions: effects of experimental conditions and electrokinetic models on the interpretation of results, *Langmuir*, 2021, **37**, 13379–13389.

55 X. Cui, J. Li, Z.-P. Zhang, Y. Fu, L. Liu and Q.-X. Guo, Pd (quinoline-8-carboxylate) 2 as a low-priced, phosphine-free catalyst for Heck and Suzuki reactions, *J. Org. Chem.*, 2007, **72**, 9342–9345.

56 S. J. Sabounchei, M. Ahmadi, T. Azizi and M. Panahimehr, A Robust, Moisture-and Air-Stable Phosphine Mono-Ylide Palladacycle Precatalyst: A Simple and Highly Efficient System for Mizoroki–Heck Reactions, *Synlett*, 2014, **25**, 336–342.

57 M. Feuerstein, H. Doucet and M. Santelli, Efficient Heck vinylation of aryl halides catalyzed by a new air-stable

palladium-tetraphosphine complex, *J. Org. Chem.*, 2001, **66**, 5923–5925.

58 C. Yang, H. M. Lee and S. P. Nolan, Highly efficient Heck reactions of aryl bromides with n-butyl acrylate mediated by a palladium/phosphine− imidazolium salt system, *Org. Lett.*, 2001, **3**, 1511–1514.

59 A.-E. Wang, J.-H. Xie, L.-X. Wang and Q.-L. Zhou, Triaryl phosphine-functionalized N-heterocyclic carbene ligands for Heck reaction, *Tetrahedron*, 2005, **61**, 259–266.

60 C. Hansch, A. Leo and R. Taft, A survey of Hammett substituent constants and resonance and field parameters, *Chem. Rev.*, 1991, **91**, 165–195.

61 D. H. McDaniel and H. C. Brown, An extended table of Hammett substituents constants based on the ionization of substituted benzoic acids, *J. Org. Chem.*, 1958, **23**, 420–427.

62 R. Ouyang, J.-X. Liu and W.-X. Li, Atomistic theory of Ostwald ripening and disintegration of supported metal particles under reaction conditions, *J. Am. Chem. Soc.*, 2013, **135**, 1760–1771.

63 J. Li, R. Hua and T. Liu, Highly chemo-and stereoselective palladium-catalyzed transfer semihydrogenation of internal alkynes affording cis-alkenes, *J. Org. Chem.*, 2010, **75**, 2966–2970.

64 R. Shen, T. Chen, Y. Zhao, R. Qiu, Y. Zhou, S. Yin, *et al.*, Facile regio-and stereoselective hydrometalation of alkynes with a combination of carboxylic acids and group 10 transition metal complexes: selective hydrogenation of alkynes with formic acid, *J. Am. Chem. Soc.*, 2011, **133**, 17037–17044.

65 H. Kato, A. Nakamura, K. Takahashi and S. Kinugasa, Accurate size and size-distribution determination of polystyrene latex nanoparticles in aqueous medium using dynamic light scattering and asymmetrical flow field flow fractionation with multi-angle light scattering, *Nanomaterials*, 2012, **2**, 15–30.

66 C. Burda, X. Chen, R. Narayanan and M. A. El-Sayed, Chemistry and properties of nanocrystals of different shapes, *Chem. Rev.*, 2005, **105**, 1025–1102.

67 R. Devivaraprasad, T. Kar, A. Chakraborty, R. K. Singh and M. Neergat, Reconstruction and dissolution of shape-controlled Pt nanoparticles in acidic electrolytes, *Phys. Chem. Chem. Phys.*, 2016, **18**, 11220–11232.

68 L. Melo, A. Hui, M. Kowal, E. Boateng, Z. Poursorkh, E. Rocheron, *et al.*, Size distributions of gold nanoparticles in solution measured by single-particle mass photometry, *J. Phys. Chem. B*, 2021, **125**, 12466–12475.

69 J.-C. Tseng, M.-Y. Wu and W.-L. Huang, Improved practical synthesis of the sex pheromone of female sweet potato weevil, Cylas formicarius, *Int. J. Appl. Sci. Eng.*, 2013, **11**, 293–300.

70 S. Mithran and A. Subbaraman, Synthesis of (3 Z)-Dodecenyl-(E)-2-butenoate, the Pheromone of Sweet Potato Weevil, *Molecules*, 1999, **4**, 159–164.